

# Perturbative regime of terahertz high-harmonic generation in topological insulators

S. Kovalev,<sup>1,\*</sup> J.-C. Deinert,<sup>1</sup> I. Ilyakov,<sup>1</sup> N. Awari,<sup>1</sup> M. Chen,<sup>1</sup> A. Ponomaryov,<sup>1</sup> M. Bawatna,<sup>1</sup> T.V.A.G. de Oliveira,<sup>2,3</sup> L.M. Eng,<sup>2,3</sup> K.A. Kuznetsov,<sup>4,†</sup> G.Kh. Kitaeva,<sup>4</sup> P.I. Kuznetsov,<sup>5</sup> and M. Gensch<sup>1,6,7</sup>

<sup>1</sup>*Helmholtz Zentrum Dresden Rossendorf, Germany*

<sup>2</sup>*Technische Universität Dresden, Germany*

<sup>3</sup>*ct.qmat - Cluster of Excellence on Complexity and Topology in Quantum Matter*

<sup>4</sup>*Lomonosov Moscow State University, Russia*

<sup>5</sup>*Kotelnikov IRE RAS, Russia*

<sup>6</sup>*DLR - Institute of Optical Sensor Systems, Germany*

<sup>7</sup>*Technische Universität Berlin, Germany*

In this Letter, terahertz high harmonic generation processes in topological insulators of the bismuth and antimony chalcogenides family are investigated. Field conversion efficiencies are determined and clean cubic and quintic power-law scaling is observed for third and fifth harmonics, up to driving terahertz fields of 140 kV/cm. This is in contrast to all previous experiments on terahertz harmonics generation in Dirac materials where a non-perturbative regime has been observed already at few 10's kV/cm driving fields [1–4]. Our nonlinear THz spectroscopy experiments are complemented by THz pump optical probe measurements showing distinctly different relaxation dynamics of the carriers in the topologically-protected Dirac states at the surfaces and the bulk. The THz-induced dynamics of surface states reveal ultrafast relaxation that prevents accumulation effects, and results in a clear perturbative regime of THz harmonics generation that is different to graphene or Dirac semimetals with their slower relaxation times in the few ps regime [3, 5].

Nowadays, due to their unique transport properties, topological insulators (TI) attract great attention [6, 7]. The surface states of TIs are metallic with a Dirac cone band structure and time-reversal symmetry protection. This makes TIs natural candidates for next generation electronic and spintronic devices [8]. The Dirac cone band structure at the interface enables efficient frequency multiplication in the GHz/THz bands, opening up exciting technological opportunities for future high frequency electronics. Very recently it was experimentally demonstrated that doped graphene, the prototype material exhibiting Dirac band structure, has exceptionally high THz nonlinearities [1]. High harmonic generation (HHG) up to the 7<sup>th</sup> order with extremely high efficiencies that exceed that of other solids by orders of magnitude has been demonstrated. The underlying process can be well described by efficient ultrafast heating and subsequent cooling of the free background Dirac fermions when interacting with THz fields [5, 9]. However, this process saturates already at relatively moderate fields of less than 20 kV/cm due to the accumulation of heat in the Dirac fermion reservoir. Recently, THz HHG up to the seventh order was observed in the  $Cd_3As_2$  3D Dirac semimetal [2, 3] revealing as well a non-perturbative regime. Earlier, Georgianni et al. [4] demonstrated strong nonlinear terahertz response in  $Bi_2Se_3$  topological insulator and signatures of THz third harmonic generation (THG) were shown. In all these works on THz HHG in Dirac materials [1–4] a non-perturbative regime was observed revealing either strong saturation, the presence of a threshold, or deviation of the generated harmonics' power law scaling from the harmonic number.

Here, we investigate the THz-driven nonlinear processes in topological insulators of the bismuth and antimony chalcogenide families, in order to elucidate whether the complex interactions between the protected Dirac band structure at the crystal surfaces with the properties of the insulating bulk in these materials have an influence on the THz HHG process. Of particular interest is here whether saturation effects of THz HHG observed in previous works can be avoided. All nonlinear THz spectroscopy measurements are performed in the time-domain, hence providing a direct and background-free quantitative access to the incident and re-emitted THz fields.

As high-field THz source for third harmonic generation (THG) we used optical rectification of near-infrared laser pulses in a lithium niobate crystal employing the tilted pulse front approach [10]. Bandpass filters were used to confine the spectral content to 15% bandwidth around a central frequency of 500 GHz. The resulting narrow-band THz pulses had a pulse energy of 150 nJ. The estimated peak field is around 100 kV/cm. To study the fifth harmonic generation (FHG) we used the superradiant accelerator-based light source TELBE [11], providing THz radiation at 300 GHz central frequency with up to 140 kV/cm peak field strength. Two 20 % bandwidth bandpass filters with 1500 GHz center frequency were inserted after the sample to suppress the fundamental intensity and thereby maximize the sensitivity for photons at the THG and FHG frequency. The experimental scheme is similar as in our previous work [1, 2] (Supplementary Note S1). The transmitted and emitted THz pulses are measured by electro-optical sampling with a 2 mm ZnTe crystal using 100 fs laser probe pulses.

Rhombohedral  $Bi_2Se_3$ ,  $Bi_2Te_3$  and  $Bi_{1.4}Sb_{0.6}Te_{1.51}Se_{1.49}$  (BSTS) films were grown on (0001)  $Al_2O_3$  substrates

by the MOVPE method at a temperature of 445 °C. The growth method is described in more detail in [12]. According to AFM measurements, the films had thicknesses of 30, 490, and 375 nm, respectively. It was shown in [13] that for topological insulators of the  $Bi_{2-x}Sb_xTe_{3-y}Se_y$  quaternary compounds, there is an optimal curve (Ren's curve) in the composition diagram  $y(x)$ . Near this curve, the properties of electronic edge states are most pronounced due to the fact that acceptors and donors mutually cancel each other out. Compositions below Ren's curve, as a rule, have predominant hole conductivity, while a composition above Ren's curve exhibits electronic conductivity. Here we investigated samples of these three cases: p-type  $Bi_2Te_3$  (490nm), n-type  $Bi_2Se_3$  (30nm), and  $BSTS$  near Ren's curve (375 nm) with the Fermi level located inside the bandgap [13–16].

In Fig. 1 the direct results of measurements of fundamental and THG fields obtained by electro-optic sampling for  $Bi_2Te_3$  as well as their amplitude spectra are shown. Similar plots for the fifth harmonic observed in  $BSTS$  are shown in the supplementary information. The THz pulses at the fundamental frequency of 500GHz have around 6-7 cycles (Fig. 1 a). The THG is clearly visible without implementing any digital filters (Fig. 1 b). To ensure that THG originates from the TI and not from the fundamental beam leakage, we replaced the sample by a  $Al_2O_3$  substrate and did not observe any THG signal at 1500 GHz. In Fig. 1 c the amplitude spectra of the fundamental beam and the THG in TI and substrate are shown.

In Fig. 2 a, the peak fields of the THG generated in  $Bi_2Se_3$ ,  $Bi_2Te_3$  and  $BSTS$  sample are plotted against the field strength of the fundamental radiation. Absolute conversion efficiencies as well as time- and frequency-domain measurements of THG are shown in the supplementary information. THz THG measurements on p-doped graphene with around  $10^{13} \text{ cm}^{-2}$  charge carrier concentration are shown for comparison. The highest conversion efficiency of about 0.5 % in field is achieved for graphene, similar to our previous work [1]. At the fundamental field strengths between 60 and 100 kV/cm the THG from graphene is strongly saturated and scales linearly with the fundamental fields. In the lowest range of driving fields, between 15 and 25 kV/cm, THG in graphene shows a power law scaling with a 2.3 slope, indicating that the perturbative regime can be reached at driving fields below 10 kV/cm already. At 100 kV/cm driving fields, the conversion efficiencies for topological insulators are 0.13, 0.08, and 0.03 % in field for  $Bi_2Te_3$ ,  $BSTS$ , and  $Bi_2Se_3$ , respectively. All topological insulators demonstrate a clean cubic dependence of the THG field meaning that THz induced nonlinear processes are far from saturation regime and further enhancement can be applied as the THG efficiency scales as fundamental field square. Note, that we have not observed any threshold for THG in the investigated TIs. The discrepancy with an observed threshold in THG [4] could be due to the non-coherent background that was measured in this work and could not be separated from THz THG using direct power transmission measurements.

In Fig. 2 b, the field strength of the fifth harmonic is shown as a function of the fundamental field strength. Here, the fundamental fields had a central frequency of 300 GHz and were generated by the accelerator-based TELBE THz facility. Due to limited beamtime at TELBE we used the  $BSTS$  sample only and observed a maximum conversion efficiency for FHG around 0.014 % at 140 kV/cm fundamental field. The observed FHG fields scale with an order of  $5.2 \pm 0.3$  with the fundamental fields, which is a clear evidence that the FHG process is in the perturbative regime. In the inset of Fig. 2 b the normalized amplitude spectra of fundamental and FHG radiation are shown, confirming the fifth order of harmonic generation.

Yoshikawa et al. [17] have demonstrated that the process of mid-IR THG in graphene reaches a maximum conversion efficiency when the fundamental beam has some finite ellipticity. In order to verify if there is any optimal pump beam ellipticity in case of THz THG we varied our pump field polarization state, changing it from linear to circular polarization using a THz quarter-wave plate and measuring the total intensity of THG as sum of p- and s-polarized waves' intensity in the  $Bi_2Se_3$  sample (see the supplementary information). We observe that THG efficiency decreases linearly with ellipticity of the fundamental beam being zero for circularly polarized pump. For a linearly polarized pump, the HHG polarization is collinear with the fundamental pump field.

In topological insulators we have not observed any deviation of THz HHG from the perturbative regime that might be associated with the ultrafast relaxation of THz-induced Dirac carrier dynamics, and thus avoiding heat accumulation effect. Nevertheless, in previous works on topological insulators it was shown that relaxation processes are not so fast for Dirac states (few ps) both for inter- [18] and intra-band [19] excitation. These timescales are similar to those in graphene, and should also result in a non-perturbative regime of THz HHG. To address this discrepancy we performed THz pump - optical reflectivity probe (TPOP) measurements of a set of topological insulators all having different Fermi levels. We attributed THz-driven slow ( $>1$  ps) relaxation dynamics to bulk states that do not contribute to the THz HHG, while Dirac surface states show an ultra-fast (few 100's fs) relaxation and are responsible for the perturbative regime of HHG observed in this work.

As probe for TPOP measurements, we used 800 nm pulses with 100 fs duration at a fluence below  $1 \mu\text{J}/\text{cm}^2$ . Probing transient reflectivity in near- or mid-IR has been used extensively to study topological insulator carrier dynamics [18, 20–23]. In these experiments, the energy of photons above or close to the bandgap was used to generate

electron-hole pairs through inter-band excitation and subsequent carrier relaxation was studied for bulk and surface states. It was demonstrated for  $Bi_2Te_3$  and  $Bi_2Se_3$  in case of excitation pulses with energy below the bandgap, that the dynamics of surface states are dominant with respect to the bulk one [24, 25]. In our work, using THz pulses with energies below 4 meV, we cannot directly induce inter-band transitions and high-field excitation results mostly in intra-band dynamics at the surface of a topological insulator and in its bulk for conducting samples. To additionally verify if the observed carrier dynamics originate from surface states (SS), bulk conduction states (BCS) or bulk valence states (BVS), we used three TIs with Fermi level in the valence band ( $Bi_2Te_3$ ), in the conduction band ( $Bi_2Se_3$ ) and inside the bandgap ( $BSTs$ ). Therefore, BCS are empty while BVS are completely filled, making intraband transitions in the bulk of  $BSTs$  Pauli blocked. For this reason, THz induced dynamics in  $BSTs$  should be dominated by excitation of surface states, while for bulk-conducting  $Bi_2Se_3$  and  $Bi_2Te_3$  intraband dynamics in bulk states is allowed.

Normalized probe pulse reflectivity changes in the set of topological insulators pumped by broadband THz radiation with 400 kV/cm field strength are shown in Fig 3. The observed dynamics are significantly different for different topological insulators and can be decomposed into several different channels: ultrafast build-up, bi-exponential decay and a Raman excited coherent phonon response. The fast rise time of THz response corresponds to ultrafast thermalization of excited carriers through electron-electron scattering. Measured with optical techniques and tr-ARPES the electron-electron scattering time constant is around 200 fs for  $Bi_2Se_3$  [26] that is several times faster than our THz driving pulse duration (several ps). The relaxation dynamics of  $Bi_2Se_3$  (Fig. 3 a) can be decomposed into two different exponential decays. The faster decay rate varies from 1.45 ps to 1.9 ps under excitation with 280 kV/cm and 400 kV/cm fields (see the supplementary information) and can be attributed to electron-phonon scattering [18]. The slowest decay channel shows a time constant of about 190 ps. The presence of a slow relaxation under sub-bandgap excitation in  $Bi_2Se_3$  was observed previously using tr-ARPES technique [24] and was attributed to thermal excitation of the carrier population.

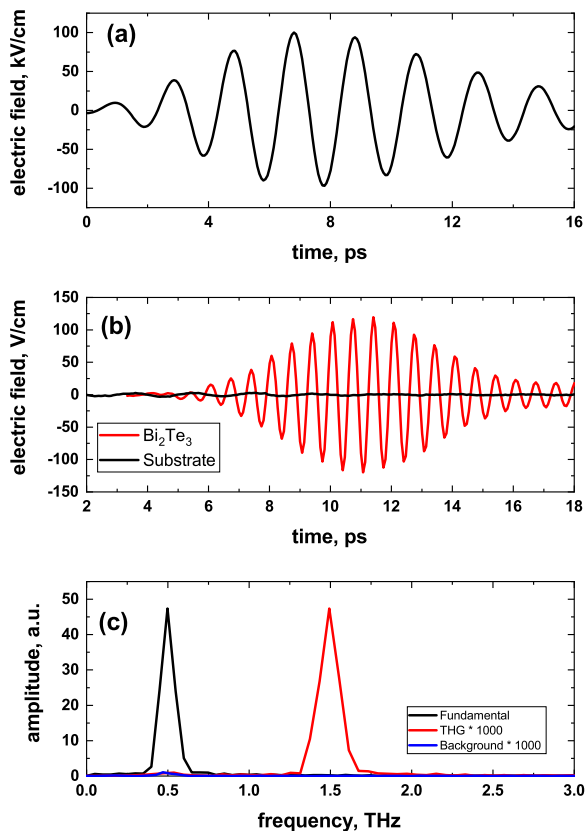


FIG. 1: Time-domain waveforms of fundamental radiation electric field (a) and the third harmonic field generated in  $Bi_2Te_3$  and  $Al_2O_3$  substrate (b). Amplitude spectra of fundamental radiation and THG in  $Bi_2Te_3$  and substrate (c).

Measurements performed on  $Bi_2Te_3$  sample are presented in Fig 3 b. Here we observed similar dynamics as for  $Bi_2Se_3$ : ultrafast carrier build-up and a slow decay. The Raman excited optical phonon is slightly redshifted (due to the heavier Te atoms) and more pronounced than in  $Bi_2Se_3$  with a center frequency around 1800 GHz (supplementary information Fig. 10). As the penetration depth of 800 nm light is about 10 nm, it is not clear if the phonon is located at the surface or if it is excited only in the bulk. The coupling between THz-driven surface state dynamics and the coherent phonon is unclear as well as its impact on the THz HHG process. To prove the origin of the coherent phonon emission from two-photon, sum-frequency excitation [27] we modified the pump pulse bandwidth and employed broad-band and narrow-band pump pulses with various central frequencies, thus controlling the spectral content at the  $A_{(1g)}$  mode frequency. The coherent Raman-active phonon at 1800 GHz is observed only in case of broad-band pump or narrow-band excitation with 1000 GHz central frequency, i.e. at around half of the  $A_{(1g)}$  mode frequency. After a sharp increase of reflectivity, the non-oscillatory part decreases within 2 ps delay time and then monotonously increases again reaching a plateau at 15 ps delay. At longer delays, the reflectivity slowly decreases with a decay time of about 600 ps (shown in the supplementary). Such dynamics are very similar to those observed for 3 eV pump excitation and are attributed to the interplay between free carrier absorption and the band filling effect [28].

Carrier dynamics in  $BSTS$  (Fig. 3 c) exhibit an ultrafast build-up following by a fast decay. The slow response that was observed in two other samples immediately after pump excitation is almost negligible. The relaxation time of  $BSTS$  is short (few 100's fs). This behaviour of THz induced charge carrier dynamics is different with respect to  $Bi_2Se_3$ ,  $Bi_2Te_3$  or with respect to  $BSTS$  dynamics induced by excitation above the bandgap [23, 29]. In all those cases, a pronounced slow relaxation is present. One possible explanation is that Fermi level of  $BSTS$  is located inside the bandgap (around 300meV) [15]. For this reason 4meV excitation can only induce dynamics of surface states while excitation of bulk states is Pauli-blocked.

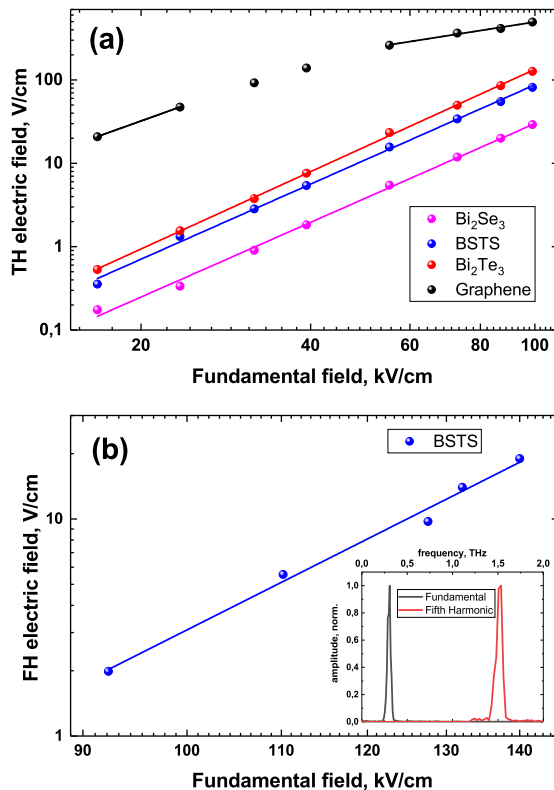


FIG. 2: (a) The peak values of third harmonic fields generated in topological insulators and graphene obtained at different driving fields of fundamental radiation at 500 GHz central frequency (dots). Solid lines are linear fits providing the scaling law:  $1.06 \pm 0.08$  for graphene at highest field and  $2.3$  at lowest fields,  $3.08 \pm 0.03$  for  $Bi_2Te_3$ ,  $2.99 \pm 0.06$  for  $BSTS$ , and  $2.98 \pm 0.07$  for  $Bi_2Se_3$ ; (b) fields of fifth harmonic generated in  $BSTS$  topological insulator, slope of linear fit is  $5.2 \pm 0.3$ ; In the inset - amplitude spectra of fundamental and fifth harmonics.

The presented results on THz HHG and TPOP in  $Bi_2Se_3$ ,  $Bi_2Te_3$  and  $BSTS$  can be well described taking into account that THz harmonics are generated at the surface of topological insulators. The excitation of surface states with few meV radiation leads to redistribution of charge carriers within Fermi level and further relaxation on a few hundreds of fs timescale due to the linear and gapless dispersion of Dirac states. Such a short relaxation time prevents accumulation effects under long narrow-band THz radiation, thus resulting in the perturbative nature of THz HHG in topological insulators. In case of bulk conducting topological insulators, the Fermi level is located inside the bulk states leading to additional excitation of bulk states with THz radiation through intraband transitions. The THz induced bulk states dynamics have a few ps relaxation time but do not contribute to the THz HHG process.

In conclusion, we have measured, for the first time to our knowledge, THz third and fifth harmonic generation in  $Bi_2Se_3$ ,  $Bi_2Te_2$  and  $BSTS$  topological insulators in time domain that allowed us to determine THz HHG efficiencies without any contributions from non-coherent processes. The power law scaling of the THG has clean cubic dependence for all samples, while for FHG a clean quintic dependence is observed, as measured in  $BSTS$ . No signatures of saturation or threshold were observed up to driving fields of 140 kV/cm, indicating the clear perturbative regime of THz HHG that is contrary to other Dirac materials, where non-perturbative regime was observed at such driving fields. It was shown for  $Bi_2Te_3$  and  $Bi_2Se_3$  that bulk metallic states contribute to the slow relaxation dynamics, while for the bulk-insulating  $BSTS$  sample the THz induced dynamics are driven through Dirac states at the surface with few 100's fs relaxation timescales. Ultrafast surface states relaxation makes accumulation effects within the long duration of the excitation pulse not efficient that results in clear perturbative regime of THz HHG. The observed perturbative regime of THz HHG in topological insulators allows one to increase the conversion efficiency further by using higher field strength of excitation or employing metamaterials to locally enhance the electric fields. The obtained results can be useful for realizing the efficient generation of higher terahertz harmonics and for various nonlinear spintronics devices based on topological insulators.

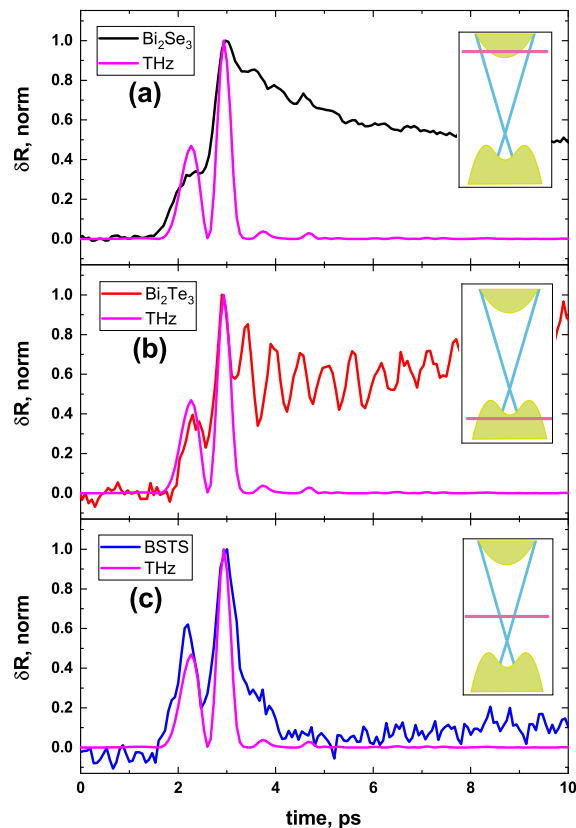


FIG. 3: THz pump Optical reflectivity probe measurements in  $Bi_2Se_3$  (a),  $Bi_2Te_3$  (b) and  $BSTS$  (c), THz instantaneous intensity of the driving field is shown for all panels (pink continuous curve). The schematic location of Fermi level (red line) against conduction and valence bands for all samples is shown in the insets.

## ACKNOWLEDGEMENTS

The authors are grateful to A.V. Shepelev for useful discussions and D.A. Safronenkov for help. Parts of this research were carried out at ELBE at the Helmholtz-Zentrum Dresden-Rossendorf e.V., a member of the Helmholtz Association. The films are grown in IRE RAS within the framework of the state task. This work was supported by the RFBR grants Nos. 18-29-20101, 19-02-00598. N.A., S.K., and I.I. acknowledge support from the European Unions Horizon 2020 research and innovation program under grant agreement No. 737038 (TRANSPIRE). T.V.A.G.O. and L.M.E. acknowledge the support by the Würzburg-Dresden Cluster of Excellence on Complexity and Topology in Quantum Matter (ct.qmat).

---

\* Electronic address: s.kovalev@hzdr.de

† Electronic address: kirill-spdc@yandex.ru

- [1] H. Hafez, S. Kovalev, J. Deinert, Z. Mics, B. Green, N. Awari, M. Chen, S. Germanskiy, U. Lehnert, J. Teichert, et al., *Nature* **561**, 507 (2018).
- [2] S. Kovalev, R. Dantas, S. Germansky, J. Deinert, B. Green, I. Ilyakov, N. Awari, M. Chen, M. Bawatna, J. Ling, et al., *Nature Communications* **11**, 2451 (2020).
- [3] B. Cheng, N. Kanda, N. Ikeda, T. Matsuda, P. Xia, T. Schumann, S. Stemmer, J. Itatani, N. Armitage, and R. Matsunaga, *Physical Review Letters* **124**, 117402 (2020).
- [4] F. Giorgianni, E. Chiadroni, A. Rovere, M. Cestelli-Guidi, A. Perucchi, M. Bellaveglia, M. Castellano, D. Giovenale, G. Pirro, M. Ferrario, et al., *Nature Communications* **7**, 11421 (2016).
- [5] H. Hafez, S. Kovalev, K. Teilrooij, M. Bonn, M. Gensch, and D. Turchinovich, *Advanced Optical Materials* **8**, 1900771 (2020).
- [6] L. Fu, C. Kane, and E. Mele, *Physical Review Letters* **98**, 106803 (2007).
- [7] A. Burkov and D. Hawthorn, *Physical Review Letters* **105**, 066802 (2010).
- [8] D. Pesin and A. MacDonald, *Nature Materials* **11**, 409 (2012).
- [9] Z. Mics, K. Tielrooij, K. Parvez, S. Jensen, I. Ivanov, X. Feng, K. Müllen, M. Bonn, and D. Turchinovich, *Nature Communications* **6**, 7655 (2015).
- [10] A. Stepanov, J. Hebling, and J. Kuhl, *Applied Physics Letters* **83**, 3000 (2003).
- [11] S. Kovalev, B. Green, T. Golz, S. Maehrlein, N. Stojanovic, A. Fisher, T. Kampfrath, and M. Gensch, *Structural Dynamics* **4**, 024301 (2017).
- [12] P. Kuznetsov, G. Yakushcheva, B. Shchamkhalova, V. Jitov, A. Temiryazev, V. Sizov, and V. Yapaskurta, *Journal of Crystal Growth* **483**, 216 (2018).
- [13] Z. Ren, A. Taskin, S. Sasaki, K. Segawa, and Y. Ando, *Physical Review B* **84**, 165311 (2011).
- [14] A. Taskin, Z. Ren, S. Sasaki, K. Segawa, and Y. Ando, *Physical Review Letters* **107**, 016801 (2011).
- [15] T. Arakane, T. Sato, S. Souma, K. Kosaka, K. Nakayama, M. Komatsu, T. Takahashi, Z. Ren, K. Segawa, and Y. Ando, *Nature Communications* **3**, 636 (2012).
- [16] S. Y. Matsushita, K. K. Huynh, H. Yoshino, N. H. Tu, Y. Tanabe, and K. Tanigaki, *Physical Review Materials* **1**, 054202 (2017).
- [17] N. Yoshikawa, T. Tamaya, and K. Tanaka, *Science* **356**, 736 (2017).
- [18] Y. Glinka, S. Babakiray, T. Johnson, A. Bristow, B. Holcomb, and D. Lederman, *Applied Physics Letters* **103**, 151903 (2013).
- [19] A. Melnikov, K. Boldyrev, Y. Selivanov, V. Martovitskii, S. Chekalin, and E. Ryabov, *Physical Review B* **97**, 214304 (2018).
- [20] J. Chen, W. Yu, P. Cadden-Zimansky, D. Smirnov, N. Tolk, I. Miotkowski, H. Cao, Y. Chen, Y. Wu, S. Qiao, and Z. Jiang, *Applied Physics Letters* **97**, 182102 (2010).
- [21] A. Wu, X. Xu, and R. Vnkatasubramanian, *Applied Physics Letters* **92**, 011108 (2008).
- [22] J. Hu, K. Igarashi, T. Sasagawa, K. Nakamura, and O. Misochko, *Applied Physics Letters* **112**, 031901 (2018).
- [23] Y. Onishi, Z. Ren, K. Segawa, W. Kaszub, M. Lorenc, Y. Ando, and K. Tanaka, *Physical Review B* **91**, 085306 (2015).
- [24] Y. Wang, H. Steinberg, P. Jarillo-Herrero, and N. Gedik, *Science* **342**, 453 (2013).
- [25] J. Reimann, S. Schlauderer, C. Schmid, F. Langer, S. Baierl, K. Kokh, O. Tereshchenko, A. Kimura, C. Lange, J. Gädde, et al., *Nature* **562**, 396 (2018).
- [26] Y. Wang, D. Hsieh, H. Steinberg, D. Gardner, Y. Lee, P. Jarillo-Herrero, and N. Gedik, *Physical Review Letters* **109**, 127401 (2012).
- [27] S. Maehrlein, A. Paarman, W. Martin, and T. Kampfrath, *Physical Review Letters* **119**, 127402 (2017).
- [28] J. Wang, L. Guo, C. Ling, Y. Song, X. Xu, Z. Ni, and Y. Chen, *Physical Review B* **109**, 127401 (2016).
- [29] Y. Choi, C. Zhung, S. Park, J. Park, J. Kim, S. Kim, J. Park, and J. Lee, *Physical Review B* **97**, 075307 (2018).